Dalton Transactions

Synthesis of $[Os(bpy)_2(py)(OH_2)](PF_6)_x$ Substituted Pyridine Complexes; Characterization of a Singly Bridged $H_3O_2^-$ Ligand

Journal:	*Dalton Transactions*
Manuscript ID	DT-ART-02-2025-000419
Article Type:	Paper
Date Submitted by the Author:	20-Feb-2025
Complete List of Authors:	Sun, Jiangtian; University of California Los Angeles, Chemistry and Biochemistry Sun, Jingwen; University of California Los Angeles, Chemistry and Biochemistry Jolly, Brandon; University of California Los Angeles, Chemistry and Biochemistry Riu, Martin; University of California Los Angeles, Chemistry Kerr, Tyler; University of California Los Angeles, Chemistry and Biochemistry Lai, Yi-An; University of California Los Angeles, Chemistry and Biochemistry Pung, Michael; University of California Los Angeles, Chemistry and Biochemistry Liu, Chong; University of California Los Angeles, Chemistry and Biochemistry Nava, Matthew; University of California Los Angeles, Chemistry and Biochemistry

ARTICLE

Synthesis of $[Os(bpy)_2(py)(OH_2)](PF_6)_x$ Substituted Pyridine Complexes; Characterization of a Singly Bridged $H_3O_2^-$ Ligand

izeReceived 00th January 20xx,
Accepted 00th January 20xx

DOI: 10.1039/x0xx00000x

Jiangtian Sun,[a] Jingwen Sun,[a] Brandon J. Jolly,[a] Martin-Louis Y. Riu,[a] Tyler A. Kerr,[a] Yi-An Lai,[a] Michael J. Pung,[a] Chong Liu*[a,b] and Matthew Nava*[a]

Proton-coupled electron transfer (PCET) underpins energy conversion processes in biological systems and fuel-forming reactions. Interrogation of the dynamics of electron and proton transfer in PCET processes requires tunable models, with synthetic transition metal aquo complexes being particularly well-explored examples. A previous study on a PCET model, $[Os^{II}(bpy)_2(py)(OH_2)]^{2+}$ (bpy = 2,2'-bipyridine; py = pyridine), reported synthetic intractability which limits access to this class of models. Herein, we report an improved protocol to synthesize a family of $[Os^{II}(bpy)_2(py)(OH_2)]^{2+}$ complexes enabling the modular tuning of the pyridine ligand (py^L) with electron-donating or -withdrawing groups on the *para*-position. The modification of the electron density about the osmium center is reflected in Hammett plots of half-wave peak potential for the Os^{II}/Os^{III} couples and pK_a values of the coordinated water. Moreover, a hydrogen-bonded osmium dinuclear structure featuring a short, strong hydrogen bonding network in the solid state was observed; we find the dinuclear Os structure is likely not maintained in solution. Our work expands access to osmium aquo complexes and provides a venue to understand how modification of supporting ligands can influence PCET processes.

Introduction

Proton-coupled electron transfer (PCET) is a chemical process involving the net transfer of a hydrogen atom (proton and electron) between a donor and acceptor.[1] The explicit pathway by which protons and electrons are transferred in PCET reactions is consequential in numerous energy conversion processes such as photosynthesis and respiration,[2–6] catalysis,[7] and homolytic bond activation.[8,9] Platforms such as small organic molecules, including phenols and quinones, as well as enzyme mimics are frequently employed to interrogate the fundamental dynamics of PCET.[10–14] However, the flexibility to tune the properties of these systems can be limited due to the extensive synthetic efforts required which pose a significant challenge for in-depth mechanistic studies, particularly when the factors governing PCET reactivity are still underdeveloped.[15,16] Therefore, it is crucial to develop a platform that features synthetic tunability, enabling the systematic investigation of molecular properties through strategic ligand selection.[17]

An exemplary system for the study of PCET processes on account of their potential for synthetic modularity and prior experimental examinations is transition metal aquo complexes (Fig. 1A).[18–20] For example, Meyer et al. reported that $[Ru^{II}(bpy)_2(py)(OH_2)]^{2+}$ would undergo successive oxidations to $[Ru^{III}(bpy)_2(py)(OH)]^{2+}$ and $[Ru^{IV}(bpy)_2(py)(O)]^{2+}$.[21] Savéant et al. synthesized the related analogue, $[Os^{II}(bpy)_2(py)(OH_2)](PF_6)_2$, and found similar oxidation behavior (Fig. 1B).[20] Kinetic analysis has indicated both the ruthenium and osmium complexes undergo concerted proton electron transfer (CPET).[20,22] Within the family of $[M^{II}(bpy)_2(py)(OH_2)]^{2+}$ complexes, controllable selection of pyridine ligands is vital for structure-function studies of supporting ligands on PCET processes and the synthetic challenges faced during the installation of a simple pyridine ligand in $[Os^{II}(bpy)_2(py)(OH_2)]^{2+}$ underscore the need for systematic investigation into the nature of the assembly of this family of complexes.

The literature synthesis of $[Os^{II}(bpy)_2(py)(OH_2)]^{2+}$ first proceeds through a reduction and ligand exchange reaction of $(NH_4)_2OsCl_6$ with bpy, yielding $Os(bpy)_2Cl_2$ (**1**, Scheme 1) followed by a salt metathesis reaction with Na_2CO_3 to produce the precursor $Os(bpy)_2CO_3$ (**2**). Treatment of **2** with acid then yields $[Os(bpy)_2(OH_2)_2]^{2+}$ (**3**), and a subsequent ligand exchange reaction with pyridine afforded the product $[Os^{II}(bpy)_2(py)(OH_2)]^{2+}$ (**4**).[20] To explore the role of the supporting ligand in PCET processes, we have targeted the modification of the pyridine ligand of **4**. To offer the largest possible scope, modification of the pyridine ligand over bipyridine was chosen due to synthetic and commercial accessibility reasons. As prepared, the pyridine and bound water of complex **4** are in a *cis* configuration, suggesting that changes in the pyridine ligand may have both an electronic and spatial influence on the water undergoing PCET.[20]

[a] Department of Chemistry and Biochemistry, University of California, Los Angeles, Los Angeles, CA, 90095, USA
[b] California NanoSystems Institute, University of California, Los Angeles, Los Angeles, CA, 90095, USA

Supplementary Information available: [details of any supplementary information available should be included here]. See DOI: 10.1039/x0xx00000x

Scheme 1. Synthetic routes for the preparation of 4-10 and line drawings of potential byproducts 11-15.

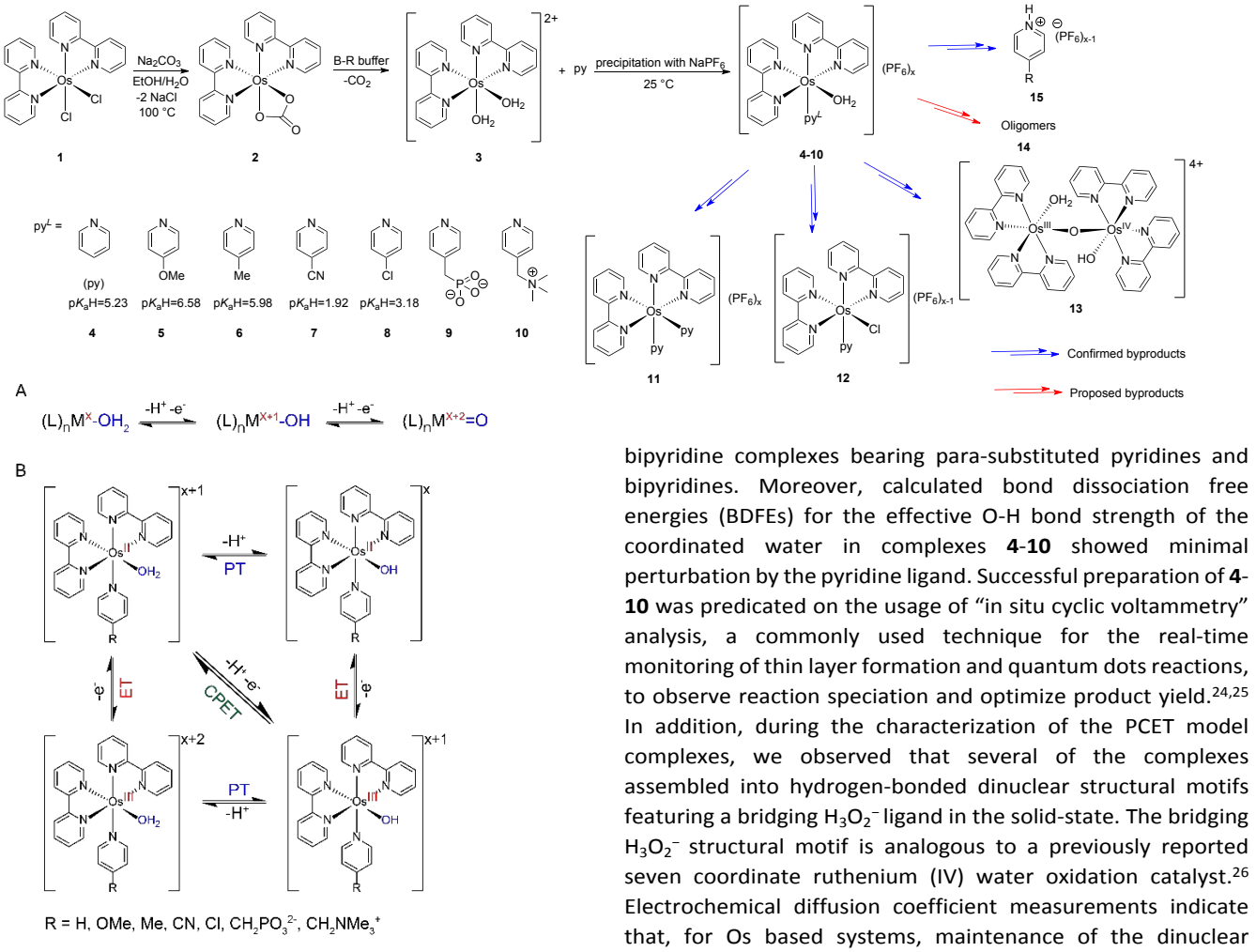

Fig. 1 A. An archetypal model for examining PCET processes **B.** Illustration of $1e^-/1H^+$ PCET square diagram of $[Os^{II}(bpy)_2(py^L)(OH_2)](PF_6)_x$ (py^L: para-substituted pyridine; PT: proton transfer; ET: electron transfer; CPET: concerted proton-electron transfer).

Herein, we report an improved procedure for the preparation of an osmium-based PCET platform (**4**) which allows for the facile access of substituted pyridine derivatives with electron-donating or electron-withdrawing groups on the *para*-position of the pyridine (Fig. 1B). To provide a modular platform for the investigation of supporting ligands in PCET processes, complexes **4**-**8**, containing pyridines of variable donating ability, and **9** and **10**, with varied overall charge, were synthesized. The synthesis of complexes **9** and **10** is of particular interest as a previously reported copper(III)-hydroxide system, bearing a charged trimethylammonium substituent, showed an anomalous rate of PCET.[23] Accordingly, the substituted pyridine derivatives **4**-**10** display a range of Os^{II}/Os^{III} redox potentials and pK_a values of the coordinated water. Plots of half-wave peak potentials and pK_a values versus Hammett constant show expected correlations and highlight the degree of electronic tunability imparted by the pyridine ligand. The resulting Hammett plots may serve as a predictive tool for estimating the redox potentials and pK_a values of other osmium aquo bipyridine complexes bearing para-substituted pyridines and bipyridines. Moreover, calculated bond dissociation free energies (BDFEs) for the effective O-H bond strength of the coordinated water in complexes **4**-**10** showed minimal perturbation by the pyridine ligand. Successful preparation of **4**-**10** was predicated on the usage of "in situ cyclic voltammetry" analysis, a commonly used technique for the real-time monitoring of thin layer formation and quantum dots reactions, to observe reaction speciation and optimize product yield.[24,25] In addition, during the characterization of the PCET model complexes, we observed that several of the complexes assembled into hydrogen-bonded dinuclear structural motifs featuring a bridging $H_3O_2^-$ ligand in the solid-state. The bridging $H_3O_2^-$ structural motif is analogous to a previously reported seven coordinate ruthenium (IV) water oxidation catalyst.[26] Electrochemical diffusion coefficient measurements indicate that, for Os based systems, maintenance of the dinuclear structure in solution is unlikely at electrochemically relevant concentrations, ruling out the possibility that the complex itself can act as the proton acceptor during PCET processes in aqueous buffer. Overall, this work establishes a readily tunable metal aquo platform for PCET mechanistic studies, where the electron density about the metal center and pK_a values of the coordinated water (proton donor) are modulated by various pyridine ligands, contributing to the advancement of synthetic strategies used to access transition metal aquo complexes. These model complexes are envisioned to serve as archetypal models for future PCET investigations.

Results and discussion

The reported method for synthesizing the PCET model, $[Os^{II}(bpy)_2(py)(OH_2)]^{2+}$ (**4**), involved heating the precursors for 2 hours, resulting in low yields (20%) and the formation of several byproducts which require tedious purification processes.[20] Through a detailed speciation analysis, we have developed an improved protocol conducted under ambient conditions which achieves not only improved yields (67±11%) without further purification, but also facile access to substituted pyridine derivatives. The precursors **1** and **2** were prepared according to literature methods and additional characterization is

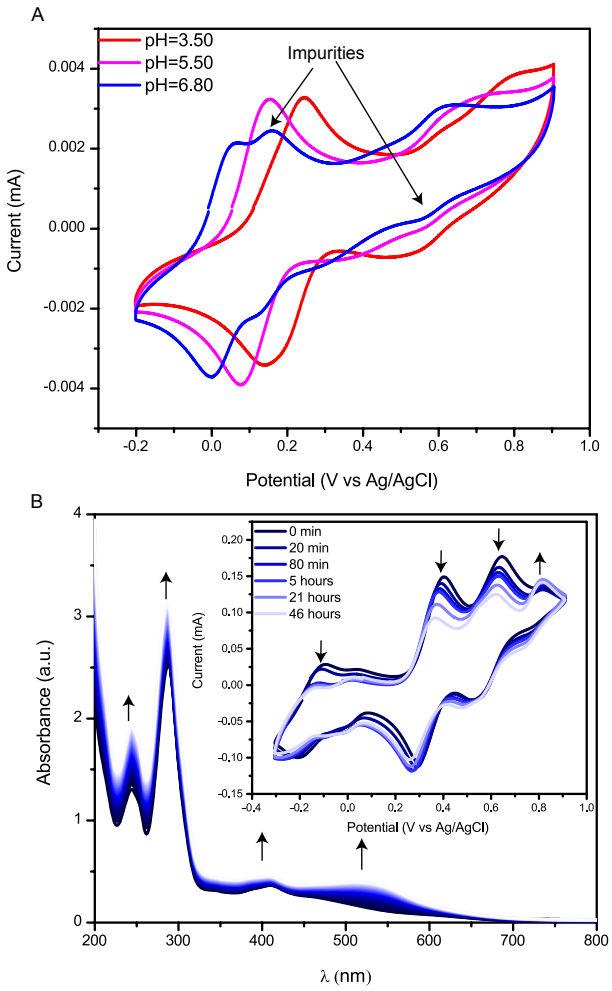

Fig. 2 A. CVs of isolated **4** at varying pH values in B-R buffer as prepared according to the literature procedure.[20] **B.** Room temperature UV-Vis spectra of **3** in B-R buffer at pH = 6.78 monitored over 20 h at half-hour intervals. Concentration of **3** = 0.74 mM; Figure inset: CVs of **3** in B-R buffer at pH = 6.80. Concentration of **3** = 17 mM. All CVs were recorded with a scan rate of 100 mV/s in B-R buffer and tested with automatic *iR* compensation.

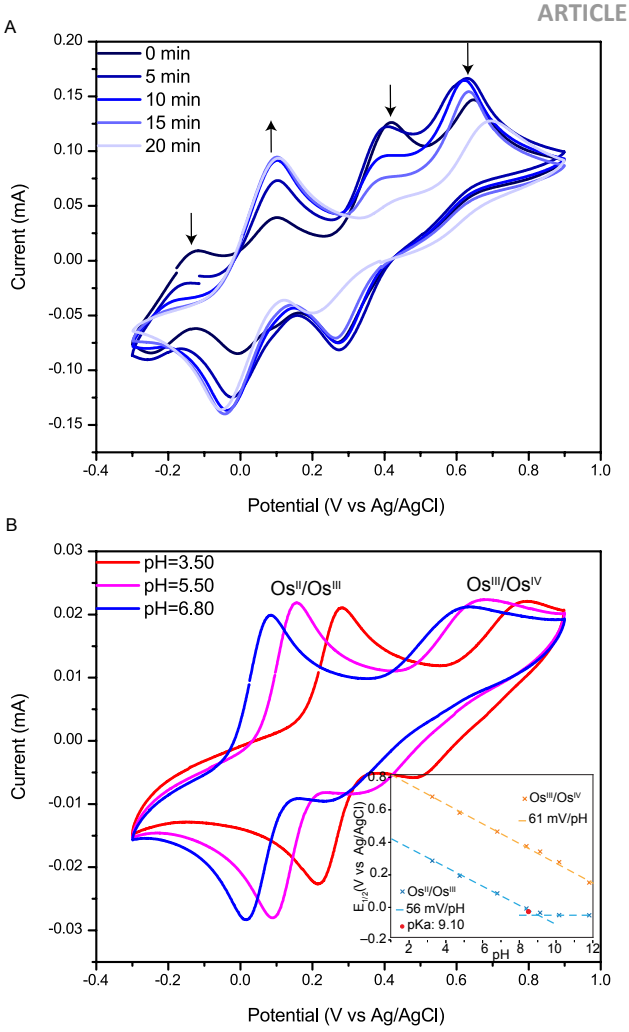

Fig. 3 A. In situ cyclic voltammetry monitoring of the reaction mixture that ultimately affords **4**. Starting concentration of **3** = 17 mM. **B.** CV traces of isolated **4**. Concentration of **4** = 2 mM. At pH 6.8: reversible waves at 0.073 ($Os^{II/III}$) and 0.433 V ($Os^{III/IV}$) vs Ag/AgCl (1 M KCl). All CVs were recorded with a scan rate of 100 mV/s in B-R buffer and tested with automatic *iR* compensation. Figure inset: Pourbaix diagram of **4** generated by variation of the apparent standard potential with pH.

documented in Sections S1 and S2.[20,27] The synthesis of compound **4** was initially reported by Savéant et al. and involved the treatment of **2** with acid affording **3** in which the waters adopt a *cis* configuration. Further treatment of **3** with pyridine (100 equiv) followed by precipitation with NH_4PF_6 yielded **4** in 20% yield.[20] The low isolated yield of **4** prompted us to evaluate the osmium speciation to improve synthetic access to the target compound with the hope that an optimized protocol would facilitate access to other pyridine derivatives. We replicated the original protocol with aqueous pH 6.80 Na_2SO_4/H_2SO_4 solution and identical amounts of pyridine followed by refluxing the reaction mixture for 2 hours. After cooling the mixture down to room temperature and precipitation with NH_4PF_6, cyclic voltammograms (CVs) of the collected precipitate redissolved in buffer indicated the presence of byproducts in the crude reaction mixture, exhibiting peaks at 0.15 V and 0.57 V vs Ag/AgCl, 1 M KCl (Fig. 2A). Notably, these peaks are unaffected by the pH of the Britton-Robinson (B-R) buffer (40 mM boric acid, 40 mM phosphoric acid, and 40 mM acetic acid), indicated the absence of coordinated water ligand(s) on the metal center.[28–30] These data suggest that the primary byproducts are likely $[Os(bpy)_2(py)_2]^{2+}$ (**11**) and $[Os(bpy)_2(py)(Cl)]^{+}$ (**12**) as inferred by cyclic voltammetry. The presence of **11** and **12** in the mixture was further confirmed by adding pyridine and NaCl into a pure B-R buffer solution of **4** (Fig. S12 and S13).

In addition to **11** and **12,** oxidization, dimerization and oligomerization products of **3** were also detected in crude reaction mixtures. Previously, $[(bpy)_2(OH_2)Os^{III}OOs^{IV}(OH)(bpy)_2]^{4+}$ (**13**) was characterized by a diagnostic peak at 513 nm in the UV-Vis spectrum which was also apparent in our reaction mixtures (Fig. 2B).[31] The loss of peaks in the CVs of solutions of **3** without pyridine indicated the formation of oligomers (Fig. 2B inset) and suggested **3** is not indefinitely stable in solution. Moreover, excess pyridine used

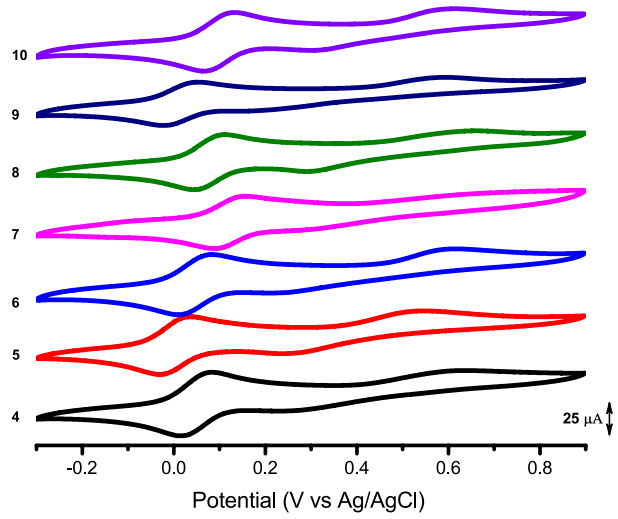

Fig. 4. CV traces of compounds **4**-**10** in B-R buffer at pH 6.8. Concentration = 2 mM. All CVs were recorded with a scan rate of 100 mV and tested with automatic *iR* compensation.

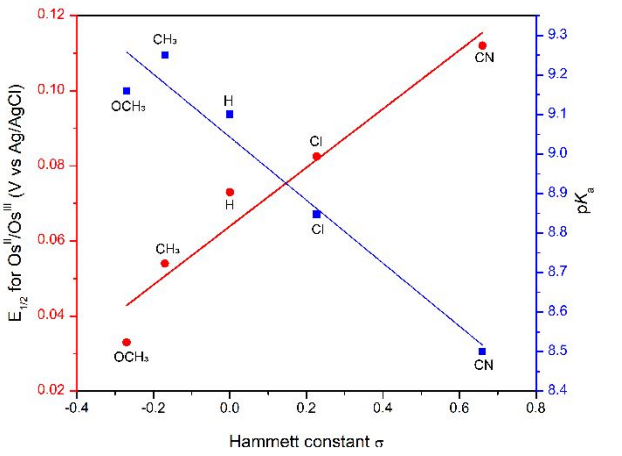

Fig. 5. Plot of the Hammett constant (σ) of the *para*-substituent on the pyridine versus $E_{1/2}$ (red trace, R^2 = 0.924, slope = +0.078) of the Os^{II}/Os^{III} couples for compounds **4**-**8**; Hammett constant (σ) versus pK_a values (blue trace, R^2 = 0.933, slope = -0.80).

Table 1. Summary of physical properties and yields for compounds 4-10.

Compound [a]	$E_{1/2}$ for Os^{II}/Os^{III} (V vs Ag/AgCl, 1 M KCl)[b]	pK_a value of coordinated water[c]	Calculated BDFE (kcal/mol)[d]	Yield (%)[e]
4 (R = H)	0.073	9.10	72.3	67±11
5 (R = OMe)	0.033	9.16	71.4	57±5
6 (R = Me)	0.054	9.25	72.0	36±8
7 (R = CN)	0.112	8.50	72.4	45±23
8 (R = Cl)	0.083	8.80	72.1	59±4
9 (R = $CH_2PO_3^{2-}$)	0.033	9.53	71.9	91 (mixed with salts)

in the formation of **4** was found to precipitate as pyridinium hexafluorophosphate (**15**) which could be observed in samples of isolated **4** by ^{1}H NMR spectroscopy (Fig. S14).

To prevent the formation of byproducts **11**-**15**, a new method for synthesizing **4** and its pyridine substituted derivatives was developed (Scheme 1). B-R buffer (pH 6.8) was identified as an ideal reaction medium as opposed to 0.1 M H_2SO_4 due to suppressed formation of **11** and other impurities (Fig. S15). In addition, NH_4PF_6 was replaced with $NaPF_6$ as the precipitation agent of **4** to avoid the formation of additional byproducts which we hypothesize to arise from NH_3 coordination to the osmium center (Fig. S16). At pH 6.8, NH_4^+ and NH_3 are in equilibrium (NH_4^+ pK_a = 9.24) and ammonia complexes of osmium are precedented.[32–34] We also reduced the amount of pyridine from 100 to approximately 20 equivalents to alleviate difficulties associated with handling the product and the partial solubility of the product **4** in pyridine. However, if less than 5 equivalents of pyridine was added to the reaction mixture, the apparent rate of conversion of **3** to **4** was significantly reduced due to lengthened reaction times and subsequent oxidation of Os(II) by O_2 affording oligomerized products (Fig. 2B, Fig. S18, and S19). To optimize the yield of **4** and minimize oligomerization of **3** at room temperature, we turned to in situ cyclic voltammetry reaction monitoring (Fig. 3A). During in situ monitoring of a typical reaction mixture at pH 6.80, peaks with $E_{1/2}$ at –0.15, 0.34 and 0.57 V vs Ag/AgCl (1 M KCl) decreased (representing the precursor **3**) while the peak with an $E_{1/2}$ at 0.073 V, (representing the product **4**) increased.

With an optimized procedure in hand, we successfully prepared complex **4** in 67±11% yield which displayed electrochemically pure CV traces without the need for crystallization (Fig. 3B). Moreover, the improved synthetic protocol for **4** allowed for the efficient preparation of complexes bearing *para*-substituted pyridines with electron-donating (**5,6**) and electron-withdrawing groups (**7,8**) in modest to high yields with slight modifications to reaction time and pyridine equivalents added. For charged pyridine derivatives $[Os^{II}(bpy)_2(py^L)(OH_2)]^x$ (R = $CH_2PO_3^{2-}$) (**9**) and $[Os^{II}(bpy)_2(py^L)(OH_2)](PF_6)_3$ (R = $CH_2NMe_3^+$) (**10**), precipitation with acetone, as opposed to the PF_6 anion, was utilized to remove unreacted **3**. Detailed synthetic procedures and characterizations of **4**-**10** are provided in Section S3. Pyridines with substituents in the *ortho*-position, such as 2-methoxypyridine, 2-*N*-(pyridin-2-ylmethyl)-*N,N,N*-trimethylammonium, quinoline, and 1,8 naphthyridine, did not yield desired products which we hypothesize is due to steric clashing (Section S4).

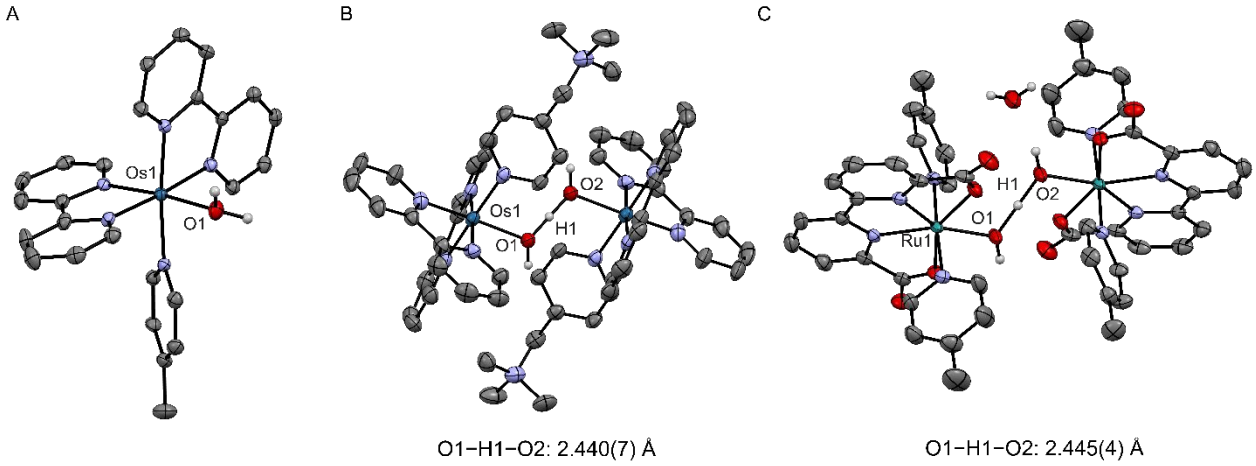

Fig. 6. Solid-state structures of: **A** mononuclear complex **6** (CCDC 2345821), **B** Complex **16** (CCDC 2366172) which was obtained through the crystallization of complex **10**, **C** seven-coordinate ruthenium (IV) water oxidation catalyst.[26] Thermal ellipsoids are plotted at the 50% probability level and all hydrogens (except for those bound to oxygens), counter ions, and solvent molecules are omitted for clarity. Selected interatomic distances [Å] and angles [deg.] for **A** Os1-O1 2.130(3) Å; **B** O1−H1−O2 2.440(7) Å, Os1-O1 2.103(4) Å, Os1-O1-O1 116.3(2)°; **C** O1−H1−O2 2.445(4) Å, Ru1-O1 1.962(2) Å, Ru1-O1-O1 117.40(1)°.

We sought to understand how varying the pyridine ligand of the complex would modulate the spectroscopic and physical properties of the coordinated water molecule. Hammett plots are often used to correlate the substituent on an organic molecule to physical properties such as redox potential and pK_a for benchmarking and prediction purposes.[35] The CVs of **4**-**10** were recorded in B-R buffer at constant pH and shown in Fig. 4. The pK_a values of **4**-**10** were determined using the Pourbaix diagram (Fig. 3B inset and Section S3) whose consistency for complex **4** was corroborated through determination via UV-Vis spectroscopic titrations (Fig. S23). A pK_a range of 8.50 (R = CN) to 9.53 (R = $CH_2PO_3^{2-}$) was observed for the complexes highlighting the degree of electronic tunability imparted by the pyridine ligand. A Hammett plot illustrating the relationship between the Hammett constant σ, $E_{1/2}$ of the Os^{II}/Os^{III} couples and pK_a values (Fig. 5) was obtained. As expected, σ and $E_{1/2}$ displayed a positive linear correlation (R^2 = 0.924, slope = +0.078) while σ and pK_a displayed a negative linear correlation (R^2 = 0.933, slope = -0.80). The magnitude of the slope in a Hammett plot provides qualitative insight as to the extent a substituent's electronic properties influence the overall physical properties or reactivity of a compound.[36] Copper aquo complexes have a positive linear correlation for plots of σ vs $E_{1/2}$, with a slope of +0.26.[23] Similarly, positive linear correlations were observed between σ vs $E_{1/2}$ for ruthenium (slope = +0.19) and manganese (slope = +0.09) based aquo complexes.[37,38] In contrast, negative linear correlations were observed between σ and pK_a for ruthenium (slope = -2.14) and manganese (slope = -2.29) complexes. Given the different solvent systems used for the measurement of thermodynamic properties, any direct comparisons between the systems in question should be approached with caution. The $E_{1/2}$ of the Os^{II}/Os^{III} couples, pK_a values, and yields for compounds **4**-**10** are summarized in Table 1. The overall trends in the Hammett plots illustrate that the pyridine ligands are able to tune the relative electron density about the osmium center and the Hammett plot may serve as a tool for predicting the redox potentials and pK_a values of other osmium aquo bipyridine complexes with para-substituted pyridines.

The bond dissociation free energy (BDFE), a key metric for assessing effective O-H bond strength, is typically determined using a thermodynamic cycle (Fig. 1B) and is governed by the formalism pioneered by Bordwell (Eq. 1):

$$\mathrm{BDFE} = 23.06E^\circ + 1.36\ \mathrm{p}K_a + \mathrm{C_G} \qquad (1)$$

where E°(V vs H_2) represents the one electron redox potential while C_G represents the free energy constant, which is 52.80 kcal/mol in water.[39,40] This formalism implies that a large BDFE may arise through either a high pK_a value of a bond in question or lowering of the reduction potential of the conjugate base of the Brønsted acid. In molecules, however, increasing the pK_a value of a bond often results in the lowering of E°, leading to minimal perturbations of the net BDFE of a bond. Thus, despite efforts to manipulate the acidity of the coordinated water molecule through variation of the pyridine ligand in **4**-**10**, the calculated BDFEs (Table 1) did not exhibit significant variability. While spectroscopic data suggested a *cis* configuration of the coordinated water and pyridine ligands, we sought to verify the geometric configurations of the complexes in a single crystal X-ray diffraction (SCXRD) study. Crystals of **6**, suitable for SCXRD studies, were obtained by layering a concentrated ethanol solution of **6** with diethyl ether in an NMR tube at room temperature for 2 days. Refinement of the diffraction data lead to a model in which the coordinated water and pyridine adopt a *cis* configuration (Fig. 6A) in support of our spectroscopic data. In addition to a hexafluorophosphate ion, a chloride counterion was also present in the lattice, likely originating from residual chloride present in compound **2**. Since very few crystals were formed from the layering protocol, we speculate that the structure in Fig. 6A may not necessarily reflect the bulk composition. Supporting this notion, inductively coupled plasma mass spectrometry (ICP-MS) analysis detects only trace levels of chloride in bulk samples of **6** (Fig. S43).

The solid-state structure of compound **10** was obtained by layering a concentrated methanol solution of **10** with diethyl

Table 2. Summary of transition metal complexes bearing $H_3O_2^-$ as a bridging ligand in the solid state.

Complexes	O-O distance (Å)	M-O distance (Å)	M-O-O angle (deg.)	Reference
$[\{Os^{II}(bpy)_2(py^L)\}_2(\mu\text{–}O_2H_3)]^{5+}$ (py^L = $NC_5H_4CH_2NMe_3^+$)	2.440(7)	2.103(4)	116.3(2)	Complex **16**, this work
$[\{W_3O_2(O_2CC_2H_5)_6(OH_2)_2\}_2(\mu\text{–}O_2H_3)]^{3+}$	2.48(1)	1.99(1)	116.5(2)	43
$[\{Mo_3O_2(O_2CC_2H_5)_6(OH_2)_2\}_2(\mu\text{–}O_2H_3)]^{3+}$	2.52(1)	2.01(1)	118.9(2)	43
cis-$[Cr^{III}(bpy)_2(\mu\text{–}O_2H_3)]_2^{4+}$	2.446(5)	1.925(3)	127.1(2)	42
trans-$[Co^{III}(en)_2(\mu\text{–}O_2H_3)]^{2+}$ (en = ethylenediamine)	2.441(2)	1.916(1)	130.4(1)	42
trans-$[Rh^{III}(terpy)(OH)(H_2O)_2]^{2+}$ (terpy = 2,2′:6′,2′′-terpyridine)	2.440(1)	1.980(2)	127.8(7)	44
cis-[(PSiP-*i*Pr)Ir^{III}(H)(OH)(H_2O)] (PSiP-R = [{2-(R_2P)C_6H_4}$_2$MeSi]$^-$)	2.587(4)	2.200(3)	97.9(1)	45
$[\{LRu^{III}(acac)\}_2(\mu\text{–}O_2H_3)]^{3+}$(L = 1,4,7-trimethyl-1,4,7-triazacyclononane, acac = acetylacetonate)	2.494(7)	2.043(4)	117.8(2)	48
trans-$[\{Ru^{III}(bpy)_2(OH_2)(OH)]^{2+}$	2.538(7)	2.007(3)	127.2(1)	49
$[\{LRu^{II}(bqdi)\}_2(\mu\text{–}O_2H_3)]^{3+}$ (bqdi = o-benzoquinone diimine)	2.459(6)	2.066(3)	124.9(2)	50
cis-$[\{Ru^{III}NO(NH_3)_2Cl_2\}_2(\mu\text{-}O_2H_3)]Cl$	2.407(3)	1.988(2)	135.0(1)	51
$[\{Ru^{IV}L(pic)_2\}_2(\mu\text{–}O_2H_3)]^{3+}$ (L = (2,2′-bipyridine-6,6′-dicarboxylic acid, pic = 4-picoline)	2.445(4)	1.962(2)	117.40(1)	26

ether in an NMR tube at room temperature for 2 days (Fig. 6B). Similar to compound **6**, the *cis* configuration of the water and pyridine ligands were observed in **10**. However, a unique intermolecular hydrogen-bonding interaction present in the structure of **10** was observed in which the oxygen of the water molecule shows an unusually short contact (2.440(7) Å, O–O distance) to another water counterpart in a neighboring unit cell. Based on the overall charge of the complex, the solid-state structure of **10** is described as an Os^{II}–OH fragment bound to a Os^{II}–H_2O with a short, strong hydrogen bond (SSHB),[41] or alternatively, the structure can be described as the symmetric $H_3O_2^-$ ligand between two osmium(II) centers. The formula of the solid-state structure derived from compound **10** is $[\{Os^{II}(bpy)_2(py^L)\}_2(\mu\text{–}O_2H_3)](PF_6)_5$ (R = $CH_2NMe_3^+$), designated as **16** for accuracy, and is the dinuclear of complex **10** but missing HPF_6. Buffer was not used during the crystallization of the complex which we speculate is crucial to the observation of deprotonation of the aquo ligand in the solid state. The non-bridging hydrogen atom of the Os–OH unit could be located from the difference Fourier map and has an angle of 116(3)° and closely matches that of the Os–O–O angle of 116.3(2)°. We were curious as to whether the other osmium pyridine aquo complexes **4**–**9** are capable of forming dinuclear structures in the solid state and conducted a SCXRD study of **6** crystalized under similar conditions that that of **16** and were able to obtain a structure exhibiting an identical dinuclear SSHB network as in complex **16** (Fig. S81). Unfortunately, severe disorder of the anion and solvent prevented the authoritative reporting of bond metrics, and thus, only connectivity can be inferred from the structure of dinuclear **6**. Nonetheless, the dinuclear structure of **6** suggests that ability of $[Os^{II}(bpy)_2(py^L)(OH_2)]^{x+}$ complexes to form SSHB networks is general.

To further corroborate the SSHB present in the solid-state structure of **10**, the strong hydrogen bonding system was analyzed by IR spectroscopy (Fig. S71), which exhibited a broad peak at 3450 cm^{-1}. Bands corresponding to O-H stretching of the coordinated water ligand were observed by IR spectroscopy for pyridine derivatives **4-10** (Section S3); however, no discernable trend in the O-H stretching frequency was observed.

Understanding hydrogen bonding interactions is crucial for interpreting the kinetics of PCET, where the identity of the proton acceptor and the distance between the proton donor and acceptor significantly influence reaction rates. According to three-phase vapor tensiometry (TPVT) results obtained by Bino et al, aqueous solutions of $[Cr(bpy)_2(OH_2)_2](NO_3)_3$, remain mononuclear until high concentrations of the metal ion are reached (120 mM) and bridging $H_3O_2^-$ is formed, whereas at a low concentration (0.5 mM), the chromium species remain as mononuclear aquo ions.[42] To evaluate whether the SSHB present in the structure of **16** is maintained in solution, we performed diffusion coefficient measurements. It was observed, based on electrochemical diffusion coefficient measurements, that compounds **4** ($D = 3.0 \pm 0.6 \times 10^{-6}$ cm^2/s) and **10** ($D = 2.8 \pm 0.8 \times 10^{-6}$ cm^2/s), whose value was corroborated by ^1H DOSY measurements (Fig. S28 and S72), displayed diffusion coefficient values invariant of their respective concentrations and the pH of B-R buffer implying that the complexes are mononuclear in solution (Tables S1 and S2).The measured diffusion coefficient values of **4** and **10** were close to that of $[Os(bpy)_3](PF_6)_2$ ($D = 3.5 \pm 0.3 \times 10^{-6}$ cm^2/s) in B-

Table 3. Summary of osmium complexes that have not been previously identified to contain bridging $H_3O_2^-$ ligands in the solid state.

Complexes	O-O distance (Å)	M-O distance (Å)	M-O-O angle (deg.)	Reference
$[Os^{III}(OH)(H_2O)(tpa)]^{2+}$(tpa = tris(2-pyridylmethyl)amine)	2.467(6)	2.062(4)	119.7(2)	52
$[Os^{III}(OH)(H_2O)(L–N_4Me_2)]^{2+}$ (L–N_4Me_2 = *N*,*N*′-dimethyl-2,11-diaza-[3,3](2,6)pyridinophane)	2.423(9)	2.029(7)	120.4(2)	53

R buffer which is incapable of intermolecularly hydrogen bonding to itself further supporting the supposition of the mononuclear nature of the osmium pyridine aquo complexes in solution (Table S3). Given that our electrochemical measurements were conducted at a low concentration (2 mM), it is likely that the osmium species remain as mononuclear in aqueous solution. Furthermore, the comparatively low solubilities of the PF_6 salts of **4**-**10** prohibit examination of their solution speciation at higher concentrations. Therefore, osmium pyridine aquo complexes showing SSHBs in the solid state may not accurately reflect the structures present in solution.$H_3O_2^-$ is a relatively rare ligand in transition metal coordination chemistry. Bino *et al*. reported the first solid-state structural evidence of a bridging $H_3O_2^-$ ligand in metal complexes, thus confirming spectroscopic results suggesting the existence of bridging $H_3O_2^-$ ligands.[43] The complexes $[\{M_3O_2(O_2CC_2H_5)_6(OH_2)_2\}_2(\mu\text{–}O_2H_3)]^{3+}$ (where M = W or Mo) display O–O distances of 2.48(1) Å and 2.52(1) Å, and M–O distances of 1.99(1) Å and 2.01(1) Å, respectively (Table 2).[43] Subsequent studies by the same group led to the discovery of two additional metal complexes containing $H_3O_2^-$ as a coordinating ligand: *cis*-$[Cr^{III}(bpy)_2(\mu\text{–}O_2H_3)]_2^{4+}$ (O–O distance of 2.446(5) Å and Cr–O distance of 1.925(3) Å) and *trans*-$[Co^{III}(en)_2(\mu\text{–}O_2H_3)]^{2+}$ (en = ethylenediamine, O–O distance of 2.441(2) Å and Cr–O distance of 1.916(1) Å).[42] *trans*-$[Rh^{III}(terpy)(OH)(H_2O)_2]^{2+}$ (terpy = 2,2′:6′,2′′-terpyridine) features an O–O distance of 2.440(1) Å and a Rh–O distance of 1.980(2) Å.[44] *cis*-[(PSiP-*i*Pr)Ir^{III}(H)(OH)(H_2O)] (PSiP-R = [{2-(R_2P)C_6H_4}$_2$MeSi]$^-$) features an O–O distance of 2.587(4) Å and a Ir–O distance of 2.200(3) Å.[45] From these studies, it can be generalized that *cis* aqua hydroxo ions typically form dinuclear complexes bridged by two $H_3O_2^-$ ligands, while *trans* aqua hydroxo ions assemble into polynuclear chains bridged by single $H_3O_2^-$ ligands. Additionally, Bino proposed that olation reactions mechanistically proceed through the elimination of water molecules from $H_3O_2^-$ bridges followed by the formation of OH bridges between the metal ions in both in the solid state and in aqueous solutions.[42] The chemistry of the $H_3O_2^-$ ligand coordinated to transition metals has branched out since Bino's original foundational research. Monge et al. studied the first metal–organic framework (MOF) that incorporates bridging $H_3O_2^-$ ligands within its structure.[46] The stabilization of $H_3O_2^-$ ligands in MOF materials introduces a new tool to address protonic conductivity and catalysis mediated by a $H_3O_2^-$ bridge.[46]

While numerous examples of metal complexes bearing the bridging $H_3O_2^-$ ligand have been uncovered, to our knowledge, a singular $H_3O_2^-$ ligand coordination to an osmium center in a terminal or bridging fashion has not been structurally identified prior to our work.[47] Comparison of the metrical parameters of **16** with that of other known complexes bearing $H_3O_2^-$ bridging ligands suggests that the $H_3O_2^-$ of **16** is unremarkable while the Os–O distance of 2.103(4) Å is quite long due the osmium's relatively low oxidation state. The hydrogen atom of the SSHB of **16** is positioned at the crystallographic inversion center between the two Os(II) units and the SSHB network bears a striking resemblance to several Group 8 octahedral ruthenium complexes in the formal II and III oxidation states. $[\{LRu^{III}(acac)\}_2(\mu\text{–}O_2H_3)]^{3+}$ (L = 1,4,7-trimethyl-1,4,7-triazacyclononane, acac = acetylacetonate) features an O–O distance of 2.494(7) Å and a Ru–O distance of 2.043(4) Å while *trans*-$[Ru^{III}(bpy)_2(OH_2)(OH)]^{2+}$ features an O–O distance of 2.538(7) Å and a Ru–O distance of 2.007(3) Å.[48,49] $[\{LRu^{II}(bqdi)\}_2(\mu\text{–}O_2H_3)]^{3+}$ (bqdi = o-benzoquinone diimine) features an O–O distance of 2.459(6) Å and a Ru–O distance of 2.066(3) Å.[50] *cis*-$[\{Ru^{III}NO(NH_3)_2Cl_2\}_2(\mu\text{-}O_2H_3)]Cl$ features an O–O distance of 2.407(3) Å and a Ru–O distance of 1.988(2) Å.[51] An outlier, from a geometric and oxidation state perspective, is the structurally characterized seven-coordinate ruthenium (IV) dinuclear $H_3O_2^-$ complex, $[\{Ru^{IV}L(pic)_2\}_2(\mu\text{–}O_2H_3)]^{3+}$ (L = (2,2′-bipyridine-6,6′-dicarboxylic acid, pic = 4-picoline), that serves as a competent homogenous water oxidation catalyst (Fig. 6C).[19] The ruthenium water oxidation catalyst system in question features a symmetric O–H···O bond and O–O distance of 2.445(4) Å, although this system displays additional waters hydrogen bonding to the dangling OH bonds of the $H_3O_2^-$ ligand. The authors speculate that the unique structural features of the dinuclear facilitate water oxidation by providing a proton transfer channel.

While scrutinizing the Cambridge Structural Database for transition metal complexes bearing combinations of OH^- and H_2O ligands, we identified three osmium complexes that, upon expansion of the crystallographic packing, revealed pairs of bridging $H_3O_2^-$ ligands in their solid-state structures. $[Os^{III}(OH)(H_2O)(tpa)]^{2+}$(tpa = tris(2-pyridylmethyl)amine) features a bridging $H_3O_2^-$ ligand with an O–O distance of 2.467(6) Å and an Os–O distance of 2.062(4) Å (Table 3).

Although this complex was reported to catalyze the stereoselective *cis*-1,2-dihydroxylation of alkenes upon oxidation by H_2O_2, the presence of the two $H_3O_2^-$ bridging ligands in the solid-state structure was not identified.[52] A similar omission of the identification of bridging $H_3O_2^-$ ligands in two other osmium aquo complexes was noted: $[Os^{III}(OH)(H_2O)(L–N_4Me_2)]^{2+}$ ($L–N_4Me_2$ = *N*,*N*′-dimethyl-2,11-diaza-[3,3](2,6)pyridinophane), featuring an O−O distance of 2.423(9) Å and an Os−O distance of 2.029(7) Å, and $[Os^{III}(OH)(H_2O)(BPMCN)]^{2+}$ (BPMCN = *trans*-*N*,*N*′-dimethyl-*N*,*N*′-bis(2-pyridylmethyl)-1,2-cyclohexanediamine) with an O−O distance of 2.457(6) Å and an Os−O distance of 2.059(4) Å. The two aforementioned complexes serve as precatalysts for the stereoselective oxidative cyclization of 1,5-dienes and the stereoselective dihydroxylation and aminohydroxylation of styrene, respectively.[53,54] All three structures have similar O−O bond lengths to that of **16** and have shorter Os−O bonds which would be expected for an Os^{III} complex. Given that osmium aquo complexes can serve as catalysts or precatalysts in numerous reactions, our structural observations suggest that it may be critical to evaluate whether dinuclear structures may persist under catalytically relevant conditions.

Conclusion

In conclusion, we have described an improved synthetic protocol to synthesize PCET models $[Os^{II}(bpy)_2(py^L)(OH_2)](PF_6)_x$. Notably, this new procedure, guided by in situ cyclic voltammetry analysis, enabled the facile synthesis of osmium complexes bearing a variety of *para*-substituted pyridine derivatives in good yield and high purity. The new complexes exhibited varied Os^{II}/Os^{III} half-wave potentials and pK_a values of the coordinated water where Hammett constant σ and half-wave peak potential displayed a positive linear correlation while σ and pK_a displayed a negative linear correlation. The obtained Hammett plot indicates the degree of electronic tunability imparted by the pyridine ligand and provides a useful reference for the design of new systems. In our SCXRD study of complex **10**, we observed a hydrogen-bonded osmium dinuclear structure featuring short, strong hydrogen bonds in the solid state (**16**), similar to a previously reported homogeneous ruthenium water oxidation system. The dinuclear $H_3O_2^-$ bridged structural motif was also present in the solid-state structure of complex **6**. These dinuclear bridged structures represent the first reported examples of osmium $H_3O_2^-$ complexes and our structural and solution studies indicate that osmium may have more complex speciation then originally appreciated which could play a role in osmium-based catalysis in water. However, electrochemical diffusion coefficient measurements suggest that the dinuclear structure is unlikely to be maintained at electrochemically relevant concentrations in the solution state for $[Os^{II}(bpy)_2(py^L)(OH_2)]^{x+}$ based systems. Overall, our work provides a promising platform for researchers to elucidate the role of supporting ligands in modulating PCET processes.

Author contributions

Jiangtian Sun: conceptualization, methodology, investigation, data curation, and writing the original draft. Jingwen Sun and Brandon J. Jolly: conceptualization, formal analysis, investigation, and data curation. Martin-Louis Y. Riu, Tyler A. Kerr, Yi-An Lai, and Michael J. Pung: formal analysis and data curation. Chong Liu and Matthew Nava: conceptualization, project administration, review and edit the original draft and supervision.

Conflicts of interest

There are no conflicts to declare.

Data availability

The data supporting this article have been included as part of the ESI.†

Crystallographic data have been deposited at the CCDC under 2345821 and 2366172.†

Acknowledgements

We thank Prof. Cyrille Costentin and Dr. Hongyuan Sheng for valuable insights and discussions, and Mr. Yin Pok Wong for the elemental analysis data. We thank Dr. TC Ong for assistance with DOSY experiments. C. L. acknowledges the financial support of National Science Foundation (CHE-2247426). Y.-A. Lai acknowledges the financial support of the Dragon Gate Project (112WGRFA0100005), Ministry of Science and Technology (MoST), Taiwan. M.N. acknowledges the startup fund from the University of California, Los Angeles and the financial support of the Jeffery and Helo Zink Endowed Professional Development Term Chair.

References

1 S. Hammes-Schiffer, Proton-coupled electron transfer: classification scheme and guide to theoretical methods, *Energy Environ. Sci.*, 2012, **5**, 7696–7703.

2 N. Nelson and A. Ben-Shem, The complex architecture of oxygenic photosynthesis, *Nat. Rev. Mol. Cell. Biol.*, 2004, **5**, 971–982.

3 C. W. Hoganson and G. T. Babcock, A metalloradical mechanism for the generation of oxygen from water in photosynthesis, *Science*, 1997, **277**, 1953–1956.

4 J. H. Alstrum-Acevedo, M. K. Brennaman and T. J. Meyer, Chemical approaches to artificial photosynthesis. 2, *Inorg. Chem.*, 2005, **44**, 6802–6827.

5 D. Gust, T. A. Moore and A. L. Moore, Solar fuels via artificial photosynthesis, *Acc. Chem. Res.*, 2009, **42**, 1890–1898.

6 V. R. I. Kaila, M. I. Verkhovsky and M. Wikström, Proton-coupled electron transfer in cytochrome oxidase, *Chem. Rev.*, 2010, **110**, 7062–7081.

7 J. L. Dempsey, B. S. Brunschwig, J. R. Winkler and H. B. Gray, Hydrogen evolution catalyzed by cobaloximes, *Acc. Chem. Res.*, 2009, **42**, 1995–2004.

8 P. R. D. Murray, J. H. Cox, N. D. Chiappini, C. B. Roos, E. A. McLoughlin, B. G. Hejna, S. T. Nguyen, H. H. Ripberger, J. M.

Ganley, E. Tsui, N. Y. Shin, B. Koronkiewicz, G. Qiu and R. R. Knowles, Photochemical and electrochemical applications of proton-coupled electron transfer in organic synthesis, *Chem. Rev.*, 2022, **122**, 2017–2291.
9 E. C. Gentry and R. R. Knowles, Synthetic applications of proton-coupled electron transfer, *Acc. Chem. Res.*, 2016, **49**, 1546–1556.
10 T. F. Markle, I. J. Rhile, A. G. DiPasquale and J. M. Mayer, Probing concerted proton–electron transfer in phenol–imidazoles, *Proc. Natl. Acad. Sci. U.S.A.*, 2008, **105**, 8185–8190.
11 C. Costentin, M. Robert and J.-M. Savéant, Concerted proton–electron transfers in the oxidation of phenols, *Phys. Chem. Chem. Phys.*, 2010, **12**, 11179.
12 I. J. Rhile, T. F. Markle, H. Nagao, A. G. DiPasquale, O. P. Lam, M. A. Lockwood, K. Rotter and J. M. Mayer, Concerted proton−electron transfer in the oxidation of hydrogen-bonded phenols, *J. Am. Chem. Soc.*, 2006, **128**, 6075–6088.
13 S. Y. Reece and D. G. Nocera, Proton-coupled electron transfer in biology: results from synergistic studies in natural and model systems, *Annu. Rev. Biochem.*, 2009, **78**, 673–699.
14 O. Lampret, J. Duan, E. Hofmann, M. Winkler, F. A. Armstrong and T. Happe, The roles of long-range proton-coupled electron transfer in the directionality and efficiency of [FeFe]-hydrogenases, *Proc. Natl. Acad. Sci. U.S.A.*, 2020, **117**, 20520–20529.
15 S. Hammes-Schiffer and J. C. Tully, Proton transfer in solution: molecular dynamics with quantum transitions, *J. Chem. Phys.*, 1994, **101**, 4657–4667.
16 S. Hammes-Schiffer, Proton-coupled electron transfer: moving together and charging forward, *J. Am. Chem. Soc.*, 2015, **137**, 8860–8871.
17 M. W. Drover, A guide to secondary coordination sphere editing, *Chem. Soc. Rev.*, 2022, **51**, 1861–1880.
18 S. J. Edwards, A. V. Soudackov and S. Hammes-Schiffer, Analysis of kinetic isotope effects for proton-coupled electron transfer reactions, *J. Phys. Chem. A*, 2009, **113**, 2117–2126.
19 R. Tyburski, T. Liu, S. D. Glover and L. Hammarström, Proton-coupled electron transfer guidelines, fair and square, *J. Am. Chem. Soc.*, 2021, **143**, 560–576.
20 C. Costentin, M. Robert, J. Savéant and A. Teillout, Concerted and stepwise proton-coupled electron transfers in aquo/hydroxo complex couples in water: oxidative electrochemistry of $[Os^{II}(bpy)_2(py)(OH_2)]^{2+}$, *ChemPhysChem*, 2009, **10**, 191–198.
21 B. A. Moyer and T. J. Meyer, Properties of the oxo/aqua system $(bpy)_2(py)RuO^{2+}/(bpy)_2(py)Ru(OH_2)^{2+}$, *Inorg. Chem.*, 1981, **20**, 436–444.
22 D. R. Weinberg, C. J. Gagliardi, J. F. Hull, C. F. Murphy, C. A. Kent, B. C. Westlake, A. Paul, D. H. Ess, D. G. McCafferty and T. J. Meyer, Proton-coupled electron transfer, *Chem. Rev.*, 2012, **112**, 4016–4093.
23 D. Dhar, G. M. Yee and W. B. Tolman, Effects of charged ligand substituents on the properties of the formally copper(III)-hydroxide ($[CuOH]^{2+}$) unit, *Inorg. Chem.*, 2018, **57**, 9794–9806.
24 M. D. Levi, Z. Lu, Y. Gofer, Y. Cohen, Y. Cohen, D. Aurbach, E. Vieil and J. Serose, Simultaneous in-situ conductivity and cyclic voltammetry characterization of li-ion intercalation into thin V_2O_5 films. *J. Electroanal. Chem.*, 1999, **479**, 12–20.
25 N. P. Osipovich, S. K. Poznyak, V. Lesnyak and N. Gaponik, Cyclic voltammetry as a sensitive method for in situ probing of chemical transformations in quantum dots, *Phys. Chem. Chem. Phys.*, 2016, **18**, 10355–10361.
26 L. Duan, A. Fischer, Y. Xu and L. Sun, Isolated seven-coordinate Ru(IV) dimer complex with $[HOHOH]^-$ bridging ligand as an intermediate for catalytic water oxidation., *J. Am. Chem. Soc.*, 2009, **131**, 10397–10399.
27 E. M. Kober, J. V. Caspar, B. P. Sullivan and T. J. Meyer, Synthetic routes to new polypyridyl complexes of osmium(II), *Inorg. Chem.*, 1988, **27**, 4587–4598.
28 S. Hammes-Schiffer, Theory of proton-coupled electron transfer in energy conversion processes, *Acc. Chem. Res.*, 2009, **42**, 1881–1889.
29 K. Cui, A. V. Soudackov, M. C. Kessinger, J. Xu, G. J. Meyer and S. Hammes-Schiffer, General kinetic model for pH dependence of proton-coupled electron transfer: application to an electrochemical water oxidation system, *J. Am. Chem. Soc.*, 2023, **145**, 19321–19332.
30 C. Costentin, M. Robert and J.-M. Savéant, Concerted proton−electron transfer reactions in water. are the driving force and rate constant depending on ph when water acts as proton donor or acceptor?, *J. Am. Chem. Soc.*, 2007, **129**, 5870–5879.
31 J. A. Gilbert, Daniel. Geselowitz and T. J. Meyer, Redox properties of the oxo-bridged osmium dimer $[(bpy)_2(OH_2)Os^{III}OOs^{IV}(OH)(bpy)_2]^{4+}$. Implications for the oxidation of water to oxygen, *J. Am. Chem. Soc.*, 1986, **108**, 1493–1501.
32 A. D. Allen and J. R. Stevens, Ammine complexes of osnium(II), *Can. J. Chem.*, 1972, **50**, 3093–3099.
33 M. Williamson, N. Moustaid-Moussa and L. Gollahon, The molecular effects of dietary acid load on metabolic disease (the cellular pasadoble: the fast-paced dance of pH regulation), *Front. Mol. Med*, 2021, **1**, 777088.
34 G. M. Coia, K. D. Demadis and T. J. Meyer, Oxidation of ammonia in osmium polypyridyl complexes, *Inorg. Chem.*, 2000, **39**, 2212–2223.
35 F. M. Wisser, P. Berruyer, L. Cardenas, Y. Mohr, E. A. Quadrelli, A. Lesage, D. Farrusseng and J. Canivet, Hammett parameter in microporous solids as macroligands for heterogenized photocatalysts, *ACS Catal.*, 2018, **8**, 1653–1661.
36 B. E. Ziegler and T. B. McMahon, Computational analysis of substituent effects and Hammett constants for the ionization of gas phase acids, *Comput. Theor. Chem.*, 2013, **1008**, 46–51.
37 S. Watabe, Y. Tanahashi, M. Hirahara, H. Yamazaki, K. Takahashi, E. A. Mohamed, Y. Tsubonouchi, Z. N. Zahran, K. Saito, T. Yui and M. Yagi, Critical Hammett electron-donating ability of substituent groups for efficient water oxidation catalysis by mononuclear ruthenium aquo complexes, *Inorg. Chem.*, 2019, **58**, 12716–12723.
38 S. K. Barman, J. R. Jones, C. Sun, E. A. Hill, J. W. Ziller and A. S. Borovik, Regulating the basicity of metal–oxido complexes with a single hydrogen bond and its effect on C–H bond cleavage, *J. Am. Chem. Soc.*, 2019, **141**, 11142–11150.
39 R. G. Agarwal, S. C. Coste, B. D. Groff, A. M. Heuer, H. Noh, G. A. Parada, C. F. Wise, E. M. Nichols, J. J. Warren and J. M. Mayer, Free energies of proton-coupled electron transfer reagents and their applications, *Chem. Rev.*, 2022, **122**, 1–49.
40 F. G. Bordwell, J. Pei. Cheng and J. A. Harrelson, Homolytic bond dissociation energies in solution from equilibrium acidity and electrochemical data, *J. Am. Chem. Soc.*, 1988, **110**, 1229–1231.
41 J. Chen, M. A. McAllister, J. K. Lee and K. N. Houk, Short, strong hydrogen bonds in the gas phase and in solution: theoretical exploration of pK_a matching and environmental effects on the strengths of hydrogen bonds and their potential roles in enzymatic catalysis, *J. Org. Chem.*, 1998, **63**, 4611–4619.

42 M. Ardon and A. Bino, Role of the H_3O_2 bridging ligand in coordination chemistry. 1. structure of hydroxoaquametal ions, *Inorg. Chem.*, 1985, **24**, 1343–1347.
43 A. Bino and D. Gibson, A new bridging ligand, the hydrogen oxide ion ($H_3O_2^-$), *J. Am. Chem. Soc.*, 1981, **103**, 6741–6742.
44 D. Inoki, T. Matsumoto, H. Hayashi, K. Takashita, H. Nakai and S. Ogo, Establishing the mechanism of Rh-catalysed activation of O_2 by H_2, *Dalton Trans.*, 2012, **41**, 4328–4334.
45 H. Fang and S. Shimada, Oxidative addition of water to Ir(I) complexes bearing a pincer-type silyl ligand, *ACS Omega*, 2022, **7**, 20237–20240.
46 R. F. D'Vries, V. A. De La Peña-O'Shea, N. Snejko, M. Iglesias, E. Gutiérrez-Puebla and M. A. Monge, H_3O_2 bridging ligand in a metal–organic framework. Insight into the aqua-hydroxo↔hydroxyl equilibrium: a combined experimental and theoretical study, *J. Am. Chem. Soc.*, 2013, **135**, 5782–5792.
47 CSD search performed October 3, 2024.
48 R. Schneider, T. Weyhermueller, K. Wieghardt and B. Nuber, Mononuclear and dinuclear ruthenium complexes containing the LRu(acac) fragment. Crystal structures of $[LRu^{III}(acac)(OH)]PF_6{\cdot}H2O$, $[\{LRu^{III}(acac)\}_2(\mu\text{-}O_2H_3)](PF_6)_3$, and $[\{LRu^{III}(acac)\}_2(\mu\text{-}O)](PF_6)_2$. Characterization of the mixed-valence species $[\{LRu(acac)\}_2(\mu\text{-}O)](PF_6)_3$ (L = 1,4,7-trimethyl-1,4,7-triazacyclononane), *Inorg. Chem.*, 1993, **32**, 4925–4934.
49 B. Durham, S. R. Wilson, D. J. Hodgson and T. J. Meyer, Cis-trans photoisomerization in $Ru(bpy)_2(OH_2)_2^{2+}$. Crystal structure of *trans*-$[Ru(bpy)_2(OH_2)(OH)](ClO_4)_2$, *J. Am. Chem. Soc.*, 1980, **102**, 600–607.
50 T. Jüstel, J. Bendix, N. Metzler-Nolte, T. Weyhermüller, B. Nuber and K. Wieghardt, Ruthenium complexes containing "noninnocent" *o*-benzoquinone diimine/ *o*-phenylenediamide($^{2-}$) ligands. Synthesis and crystal structure of the nitrido-bridged complex $[\{LRu(o\text{-}C_6H_4(NH)_2)\}_2(\mu\text{-}N)](PF_6)_2{\cdot}3CH_3CN{\cdot}C_6H_5CH_3$, *Inorg. Chem.*, 1998, **37**, 35–43.
51 V. Vorobyev, V. A. Emelyanov, I. A. Valuev and I. A. Baidina, Nitrosyl *cis*-dichlorodiammine ruthenium complex with bridging $H_3O_2^-$ ligand, *Inorg. Chem. Commun.*, 2017, **76**, 40–43.
52 H. Sugimoto, K. Kitayama, S. Mori and S. Itoh, An osmium(III)/osmium(V) redox couple generating $Os^V(O)(OH)$ center for *cis*-1,2-dihydroxylation of alkenes with H_2O_2: Os complex with a nitrogen-based tetradentate ligand, *J. Am. Chem. Soc.*, 2012, **134**, 19270–19280.
53 T. Fujimoto, H. Sugimoto, K. Kai, K. Maeda and S. Itoh, Oxido-Hydroxido- and oxido-aminato-osmium(V) complexes with a cyclohexanediamine-based tetradentate ligand as active oxidants for dihydroxylation and aminohydroxylation of alkenes, *Eur. J. Inorg. Chem.*, 2019, **2019**, 2891–2898.
54 H. Sugimoto, T. Kanetake, K. Maeda and S. Itoh, Oxidative cyclization of 1,5-dienes with hydrogen peroxide catalyzed by an osmium(III) complex: synthesis of *cis*-tetrahydrofurans, *Org. Lett.*, 2016, **18**, 1246–1249.

Data availability statement (included in main text):

The data supporting this article have been included as part of the ESI.†

Crystallographic data have been deposited at the CCDC under 2345821 and 2366172.†